The Journal of Chemical Physics

RESEARCH ARTICLE | APRIL 04 2024

Characterizing the shear response of polymer-grafted nanoparticles

Special Collection: Polymer Nanoconfinement

Arman Moussavi ; Subhadeep Pal ; Zhenghao Wu ; Sinan Keten

J. Chem. Phys. 160, 134903 (2024)
https://doi.org/10.1063/5.0188494

AIP Publishing

The Journal of Chemical Physics ARTICLE pubs.aip.org/aip/jcp

Characterizing the shear response of polymer-grafted nanoparticles

Cite as: J. Chem. Phys. 160, 134903 (2024); doi: 10.1063/5.0188494
Submitted: 21 November 2023 • Accepted: 18 March 2024 •
Published Online: 4 April 2024

Arman Moussavi,[1] Subhadeep Pal,[1] Zhenghao Wu,[2] and Sinan Keten[1,3,a)]

AFFILIATIONS

[1] Department of Civil and Environmental Engineering, Northwestern University, Evanston, Illinois 60208, USA
[2] Department of Chemistry, Xi'an Jiaotong Liverpool University, Suzhou, People's Republic of China
[3] Department of Mechanical Engineering, Northwestern University, Evanston, Illinois 60208, USA

Note: This paper is part of the JCP Special Topic on Polymer Nanoconfinement.
[a)]**Author to whom correspondence should be addressed:** s-keten@northwestern.edu

ABSTRACT

Grafting polymer chains to the surface of nanoparticles overcomes the challenge of nanoparticle dispersion within nanocomposites and establishes high-volume fractions that are found to enable enhanced material mechanical properties. This study utilizes coarse-grained molecular dynamics simulations to quantify how the shear modulus of polymer-grafted nanoparticle (PGN) systems in their glassy state depends on parameters such as strain rate, nanoparticle size, grafting density, and chain length. The results are interpreted through further analysis of the dynamics of chain conformations and volume fraction arguments. The volume fraction of nanoparticles is found to be the most influential variable in deciding the shear modulus of PGN systems. A simple rule of mixture is utilized to express the monotonic dependence of shear modulus on the volume fraction of nanoparticles. Due to the reinforcing effect of nanoparticles, shortening the grafted chains results in a higher shear modulus in PGNs, which is not seen in linear systems. These results offer timely insight into calibrating molecular design parameters for achieving the desired mechanical properties in PGNs.

I. INTRODUCTION

Harnessing the synergy between polymer traits, such as mechanical properties and processability, and the multifunctionality unlocked by nanoparticles, polymer nanocomposites emerge as dynamic materials, open to meticulous refinement and enhancement.[1–5] Realization of the improvements to be made in material properties hinges on the controlled dispersion of nanoparticles within the polymer matrix.[2,6] A well-established method to answer this challenge is grafting polymer chains onto the surface of nanoparticles to obtain a well-dispersed material system.[3] Grafted polymer chains allow for the construction of polymer brush regions regulated by factors such as grafting density and polymer molecular weight.[7,8] The brush regions have manipulable attributes, such as stiffness, which gives the ability to control the positions of nanoparticles with respect to one another.[9,10] It is necessary to have a thorough understanding of the alterable parameter space available to predict and design polymer-grafted nanoparticle (PGN) materials with optimized mechanical reinforcement.

Molecular dynamics simulations are a commonly used tool in investigating the mechanical properties of polymer nanocomposite systems. All-atom molecular dynamics (AA-MD) simulations can accurately and precisely address local chain dynamics and failure mechanisms.[11] However, most AA-MD cannot access the time scale necessary for practical application molecular-level design. To overcome this spatiotemporal limitation, coarse-grained molecular dynamics (CG-MD) merges clusters of atoms into larger, coarse beads, with effective interactions derived from atomistic molecular dynamics (AA-MD) simulations.[6,12–14] With a more accessible and practical spatiotemporal scale, the structures, mechanical properties, and chain dynamics of bulk material systems can be observed.[13,15–21] Generic bead-spring models, such as those modified from the Kremer and Grest (KG), can describe the physical behavior of linear polymer chains well.[17,22] Modeling KG chains grafted onto nanoparticles is a technique that has been previously utilized and should give insight into the behavior of PGNs in a qualitative manner.[23]

While great effort has been made to characterize the mechanical properties of PGN materials through computational and

experimental means, the large alterable parameter space and intricacy in design leave gaps that must be addressed. Previously, shear modulus has been characterized experimentally for PGN materials well above their glass transition temperatures.[3,20,24] In particular, oscillatory shear measurements find enhancement in storage modulus (G') in lower frequency ranges.[25] Additionally, a stress overshoot behavior is observed in the shear response[3] and characterized through modeling techniques above glass transition temperature for polymer melts filled with PGNs[26] as well as polymer melts with free nanoparticles.[27] However, the origin of this behavior and the effects of various design parameters of PGNs on the shear response remain poorly understood.

This study aims to utilize KG coarse-grained molecular dynamics simulations to bridge this knowledge gap concerning the effects of deformation rate, grafted chain length, and nanoparticle core size on the shear mechanical properties of PGNs below their glass transition temperature. Systematic characterization of the shear modulus presented herein expands upon prior efforts that characterized properties below glass transition temperature, such as tensile strength and toughness,[3,28] and offers new insights for designing PGNs.

The methods used to model the PGN systems of this study are presented along with the equilibration as well as deformation simulation details. The focus of these results is on the shear modulus of the tested system, derived from shear deformation simulations. Using wide variation in the parameter space, the roles of deformation rate, grafted chain length, and nanoparticle core size on the shear modulus are analyzed. Chain conformations are analyzed to gain physical insight into what may cause the trending behavior. Finally, due to the intricate coupling effect of the polymer length and nanoparticle size, a relationship between the volume fraction of nanoparticles and the shear modulus of PGNs (Φ_{NP} vs G) is investigated to yield more tangible explanations.

II. SIMULATION METHODS

A. Modeling

Molecular dynamics simulations are carried out using the Large-scale Atomic/Molecular Massively Parallel Simulator (LAMMPS).[29] The Kremer–Grest model is employed with finitely extensive nonlinear elastic (FENE) chains. Spherical PGNs are constructed with three types of beads. A diagram of the anatomy of a PGN is shown in Fig. S1 of the supplementary material. The first type of bead is one core bead placed at the center of the nanoparticle. The second type of bead is the surface bead placed at a fixed radial distance from the core bead. The surface beads are placed using the Fibonacci sphere algorithm to create an evenly distributed surface. The number of surface beads corresponds to the number of polymer chains grafted to the nanoparticle as they are the respective starting point for each grafted polymer chain. The third type of bead is a polymer bead used to construct the grafted chains. The FENE polymer chains are attached on one end to the spherical nanoparticle. These chains are initially generated using a commonly employed self-avoiding random walk algorithm originating at the nanoparticle surface.[6,12,30]

It is important to highlight that all measurements are presented in terms of reduced Lennard-Jones units, where σ represents length and τ represents time. Kremer and Grest have provided a method to map the reduced units to real units.[22] They map the simulated KG polymer to the experimental work through the determined entanglement length (N_e), persistence length, and bead frictions. The diffusion data of the KG polymer model with $N_e = 35$ closely aligns with the diffusion data of polyethylene (PE) determined by nuclear magnetic resonance (NMR). The analysis by Kremer and Grest revealed that one monomer in the KG model corresponds to approximately three monomers in polyethylene (PE) when comparing the molecular weights of the polymer systems. As a result, they present a length scale mapping of 1 σ = 0.51 nm for PE. The time scale mapping is determined by correlating the Rouse diffusion constant with the corresponding value determined for the KG polymer at the equivalent number of monomers. Subsequently, the time scale mapping to PE is calculated to hold a conversion of 1 τ = 6.6 ps. It is critical to note that mapping a KG system result is heavily dependent on the characteristics of the polymer under investigation. The example mapping to PE serves purely demonstrative purposes. The comprehensive mapping of the findings of this study to a real unit system is beyond the scope of this research and heavily contingent upon the specific polymer of interest and, therefore, will not be addressed.

The grafting density of each nanoparticle is held as a constant of 0.5 ($chains/\sigma^2$) (chains per surface area). The nanoparticle core radius and grafted chain length are systematically varied to sample a large parameter space. Nanoparticle radii (R) of 1, 2, 3, 5, and 8 (σ) are tested throughout this study. PGNs with polymer chain lengths (N) of 20, 50, 100, 150, and 200 monomers are tested for each nanoparticle radius, totaling 25 systems to encompass the nanoparticle radius and chain length sample space. This study samples both the unentangled and entangled regimes for the particular polymer model used. The entanglement length of the KG polymer is approximated to be roughly 35 monomers ($N_e \approx 35$).[22,31,32] Each system configuration consists of 32 PGNs initially arranged in a face-centered cubic (FCC) Bravais lattice (Fig. 1), offering an efficient packing structure. Additionally, PGNs of similar topological parameters have been observed to fall into FCC structures in previous experimental work.[33–36] The periodic boundary conditions are set along the x, y, and z directions to simulate a continuous material system.[11,12,37]

B. Force field description

This study utilizes a modified version of the Kremer–Grest (KG) polymer model[22] as a coarse-grained approach for polymer chains to capture the general polymer mechanics. These linear polymer chains are depicted as a bead spring model. The KG polymer chain consists of (N) monomers (beads) aligned in a sequence connected by anharmonic springs. The interaction between the monomers is modeled with a FENE potential [Eq. (1)],[22]

$$E = -0.5KR_0^2 \ln\left[1 - \left(\frac{r}{R_0}\right)^2\right] + 4\varepsilon\left[\left(\frac{\sigma}{r}\right)^{12} - \left(\frac{\sigma}{r}\right)^{6}\right] + \varepsilon, \quad (1)$$

where the force constant (K) is set as 30 (ε/σ^2), the equilibrium bond distance (R_0) is 1.5 (σ), and $\sigma = \varepsilon = 1$ for the Lennard-Jones potential for non-bonded monomer–monomer interactions, which have been parameterized before.[38] All of the parameters and results reported herein for length, energy, mass, and time are presented in reduced units of σ, ε, m, and τ, respectively. Bond angles use the harmonic angle style with force field coefficients of 5-ε and 120° for

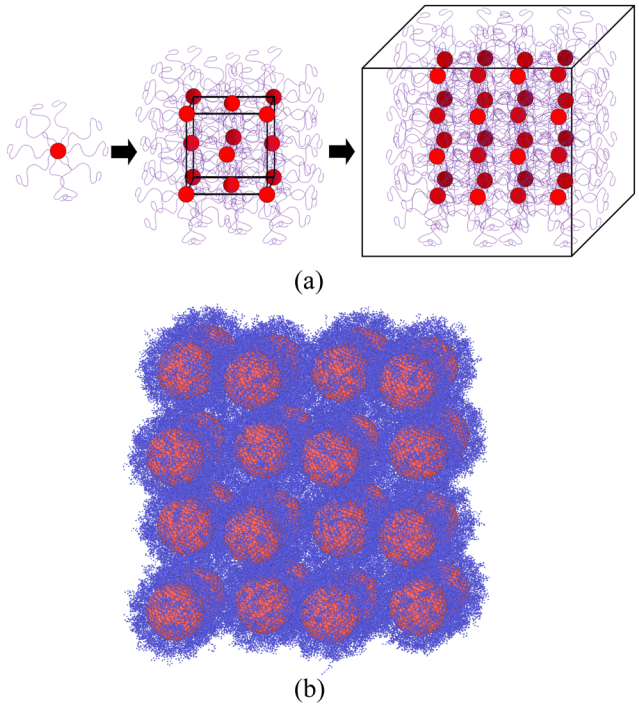

FIG. 1. PGN system initial configuration built by arranging singular polymer grafted nanoparticles into an FCC unit cell and then extending the packing with 32 PGNs: (a) graphical representation and (b) simulation configuration.

all polymer chain element prefactors and equilibrium angle values, respectively. The harmonic angle potential is selected to increase the stiffness of the chain and decrease its entanglement length, which allows for more entangled polymer melts with fewer polymer beads.

A nanoparticle is treated as a rigid body in this system due to the stark difference in stiffness relative to polymeric materials.[12,39] The fix *rigid/nvt* in LAMMPS is enforced for nanoparticle bead interactions, while integrating in a constant NVT ensemble with the Nosé–Hoover thermostat.[40] The nanoparticle is modeled as a hollow, rigid shell with a center point using two bead types as mentioned in Sec. II A. A Lennard-Jones (LJ) interaction site is positioned at the center of the nanoparticle using the core bead location (center). A shift factor is applied to the LJ potential, selected as the radius of the nanoparticle (R_{NP}), to prevent polymer beads from entering the excluded volume of the nanoparticle shell. The surface beads, located at the radial distance $d = R_{NP}$ from the center (core) bead, hold LJ interaction sites with no shift factor. Prior research has demonstrated that a lack of free volume resulting from high grafting densities on nanoparticles poses a significant challenge to the interaction of their grafted polymer chains with neighboring nanoparticles. The interactions between dense polymer coronas of even low chain length PGNs make it impossible for a neighboring nanoparticle to penetrate another nanoparticle.[15] Therefore, nanoparticle–nanoparticle (NP–NP) interactions are excluded to reduce the computational cost. However, systems with significantly lower grafted densities than what is used in this study should consider the possibilities of NP–NP interactions. Additionally, self-interactions between the nanoparticle surface beads and surface beads to center beads are set to none indicating their pairwise forces, and energy computations are excluded.

C. System equilibration

To reach the minimum energy configuration, a previously developed equilibration protocol is utilized.[6,15] A soft interatomic cosine potential is applied for a short duration to push any overlapping beads. After the short push-off simulation, the FENE potential is activated for a series of short NPT simulations, starting at high pressure and intermittently reducing the pressure to allow the system to hold its new configuration. This step is necessary to reduce the free volume within the simulation box and allow interpenetration between neighboring PGNs. Next, a long equilibration is conducted for roughly 13 000 000 time steps. A time step size of 0.01 (τ) was employed following widely accepted time step values commonly used in simulating the KG coarse-grained polymer model.[41–44] The Nosé–Hoover thermostat and barostat are applied to control the temperature and pressure of the simulation during the equilibration. The damping frequencies of the thermostat and barostat are 1.0 (τ) and 1.0 (τ), respectively. A bond-swapping technique is employed to accelerate the equilibrations of the long polymer melts. This technique enables polymer bonds to exchange positions with one another, thus preventing chains from becoming trapped in specific configurations.[45,46] The bond swapping is implemented using the LAMMPS fix *bond/swap* command.[46] Specifically, the attempted bond swapping is set at every ten steps with 0.5 fraction of polymer beads to consider for swapping and a cutoff distance of 1.3 (σ).

The full equilibration of the system is determined by monitoring chain conformations along the simulation. Once the normalized mean squared internal distance (MSID) of chains is found to converge, the systems are considered well-equilibrated.[47] Next, a quench simulation is run to replicate the annealing process as well as remove any residual stresses within the system. Through the quench simulation, the temperature is brought to 0.4 (T^*, reduced temperature unit), which is found to be below the glass transition temperature of KG polymer melts.[48] The reduction in temperature from 1 (T^*) to 0.4 (T^*) occurred over a series of simulations totaling 600 000 time steps or 6000 (τ). The systems are equilibrated at their final temperature for 200 000 time steps or 2000 (τ). Prior to the quench simulations, the FENE bond potential is substituted with a quartic bond potential. This potential facilitates bond breaking in polymer chains that are heavily stretched. The specific bond parameters utilized are adapted from the previous work on glassy polymer mechanics.[49] Figure S2 of the supplementary material illustrates the parameterization of the quartic potential compared to the FENE potential. The parameterization matches the quartic equilibrium bond length with that of the FENE bonds, while permitting the fracture of bonds upon surpassing their cutoff length. The employed force required to rupture bonds has been demonstrated in several prior studies to hold a realistic ratio to the fracture of covalent bonds found in typical polymers.[17,50–52] The application of this bond potential change protocol in addition to the parameterization of the bond potentials has been widely employed throughout the literature to study KG polymer deformation simulations.[49,53–57]

Throughout the equilibration process, the positions of the PGNs may deviate from the original FCC lattice. The deviation is dependent on the size of nanoparticles as well as the length of the grafted chains. Figure S3 of the supplementary material shows the nanoparticle radial distribution functions of fully equilibrated large and small chain lengths and nanoparticle systems. Throughout their equilibration, systems with small nanoparticles transition into an arrangement similar to that of a melt, exhibiting a disordered distribution of nanoparticles within their long-range structure. Larger nanoparticle systems shift slightly; however, they tend to remain close to their ordered FCC packing structure. These results are in line with the experimental observations regarding the effects of structural parameters on the assemblies of PGNs.[58] An ordered configuration is not well maintained as the volume of relaxed polymer chains overcomes the available void space offered in FCC packing. The decrease in nanoparticle size facilitates a reduced available void space for relaxed polymer chain segments. As the grafted polymer chain length of these systems increases, the volume of relaxed polymer ends tends to overwhelm the available space, therefore, reducing their ability to maintain a well-ordered arrangement.

The volume fraction of nanoparticles (Φ_{NP}) and monomer densities (ρ_{mon}) of each fully equilibrated system are presented in Table S1 of the supplementary material. Three distinct trials are run for each system to obtain a statistical average. The individual trials are distinguished by different lengths of additional simulation in the NPT ensemble after the system is sufficiently equilibrated. This allows the equilibrated system to explore different initial configurations for the proceeding shear deformation simulations.

D. Shear deformation

Following the full equilibration and quench of each system, a shear deformation simulation is conducted. The quartic bond style is utilized to allow bond breaking in polymer chains that are heavily stretched. It should be noted that irreversible bond breaking was not observed within the specific small strain region of interest of this study. However, integrating this aspect into the model is valuable in maintaining a physically accurate representation of the potential of mechanical failure. In the case of larger deformation, simulations must retain the capability for bond breaking to accurately capture the mechanics of failure in polymer chains.

The simulation box is switched to triclinic (non-orthogonal) to allow for six adjustable dimension parameters (x, y, z, xy, xz, and yz) for shear deformation. The shape of the simulation box is changed at a constant engineering shear strain rate using the fix deform LAMMPS command to model the shear deformation. The deformation in this scenario is small so no box flipping is enforced. The nonequilibrium molecular dynamics shear deformation simulation implements the use of the SLLOD equations of motion.[59] The fix *nvt/sllod* command is used to regulate the temperature of the system through a Nosé–Hoover thermostat and update polymer particle positions and velocities each time step. The atom positions are not remapped throughout the simulation; however, velocities are remapped when the atoms cross periodic boundaries. This technique is used to maintain a consistent velocity profile to align with the changing box shape. Similar simulation techniques reported in previous studies have been used to characterize shear deformation responses up to large strains.[27] The time step employed for all shear deformation simulations remains consistent with the time step utilized during system equilibration [0.01 (τ)]. This selection is informed by a study conducted by Lee and Kremer, which revealed negligible effects of different time step sizes on the stress autocorrelation function.[43] This finding suggests that small variations in the time step size have a minimal impact on the dynamics of the KG system. The number of time steps used for shear deformation simulation is dependent on the maximum strain desired, strain rate, and time step. Throughout the simulation, the strain is monitored using the following equation, where L_0 is the initial length of the simulation box (σ), $\dot{\gamma}_{xy}$ is the strain rate, t is the time step, and dt is the time step size:

$$\gamma_{xy} = \frac{L_0 \cdot \dot{\gamma}_{xy} \cdot t \cdot dt}{L_0}. \tag{2}$$

The virial stress tensor is calculated and collected during the shear simulations. Given that the shear deformation is applied on the xy plane, the xy component of stress (p_{xy}) becomes the focal point of this study. Once the shear deformation simulation is completed, p_{xy} is plotted as a function of the measured strain to obtain the PGN shear stress vs shear strain curves.

III. RESULTS AND DISCUSSION

A. Shear stress–strain

Figure 2 shows a sample stress–strain curve in which the system containing PGNs with nanoparticle radii of 1 (σ) is strained till 20 (σ/σ) at a rate of 0.01 (τ^{-1}). The legend provides labels corresponding to the curves plotted, differing by grafted chain lengths (N) for different nanoparticle radii of 1 (σ) systems. The simulation shown in Fig. 2(a) is observed to reach a steady shear condition at a large strain of roughly 13 (σ/σ). These systems hold nanoparticles of radii 1 (σ) and chain lengths of 20, 50, 100, 150, and 200 (N). It is important to clarify that the large strain simulation was performed for primarily illustrative purposes to demonstrate the system response to a significant strain. Analysis of the large strain response is not addressed in this study and left for future work. The focus of this work remains in the small strain region. All other systems were deformed only to a strain sufficient for observing the small strain response to avoid unnecessary computational expense. It should additionally be noted that in the region of small strain under analysis, there were no observed instances of bond breaking.

The results of this study focus on characterizing the material shear modulus, obtained by examining the small strain region of the stress–strain curve. The simple shear simulations are conducted under constant shear rates. However, it is expected that rate-dependent terms may have effects, particularly at the elevated strain rates examined within this work. Analysis is conducted for each simulation to extract the shear modulus (G) using the linear portion of the small strain region in the stress–strain curve. Figure 2(b) shows a zoomed-in image of the stress–strain curve in the small strain region. A linear function is fitted to the data of up to 2% total strain following the criteria of the previous simulation work.[60] The method of least squares is used to derive the slope of the fitted function. This slope represents the shear modulus (G) within

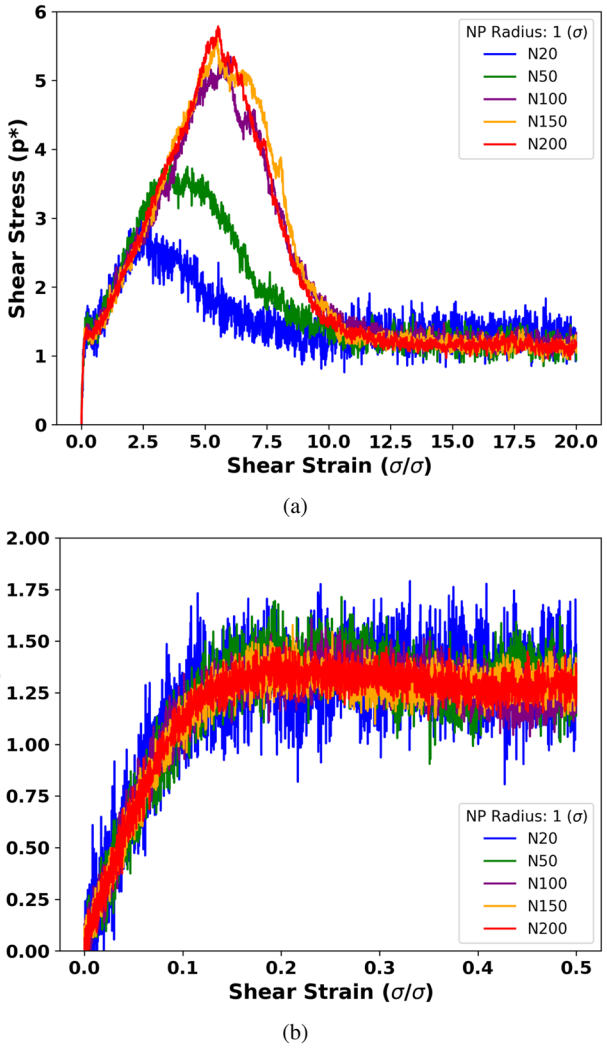

FIG. 2. Shear stress as a function of shear strain for (a) the large strain and (b) the small strain (zoomed-in view).

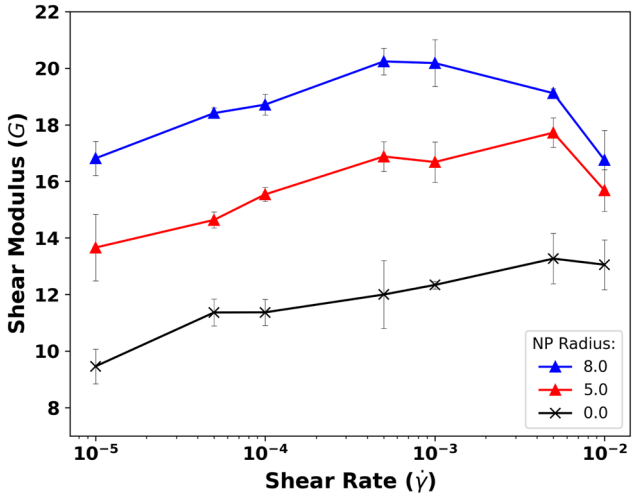

FIG. 3. Effect of strain rate on G at a constant chain length (N = 20).

this study. For each system, G is reported as a statistical average over the three trials performed to provide statistical error.

B. Strain rate dependency

Initially, the relationship between the shear rate $(\dot{\gamma})$ and G is analyzed for systems of pure linear chains and grafted nanoparticles. Figure 3 shows G as a function of shear rate for pure linear chain and grafted chains of length 20 (N). Only the selected grafted systems with a nanoparticle core radius of 5 and 8 (σ) are plotted to visualize the trending behavior for clarity. However, these trends are consistent and representative of the behavior of all nanoparticle radius systems and chain lengths, which are shown in Fig. S4 of the supplementary material.

Shear deformation simulations are conducted at seven different strain rates [0.01, 0.005, 0.001, 0.0005, 0.0001, 0.000 05, and 0.000 01 (τ^{-1})]. The results indicate that an increased strain rate generally produces a higher observed G (see Fig. S4). This relationship breaks down as strain rates surpass 0.005 (τ^{-1}). At these relatively high strain rates, the decrease in G is expected to be largely a result of the relatively high corresponding error of these points. Larger shear strain rates experience heightened noise in the simulation results due to the constant time step size across all deformation simulations. Previous simulation studies report similar observations as well as potential instabilities at large shear rates.[61] In general, the error for shear strain rates of PGNs less than 0.005 (τ^{-1}) is lower than that for higher shear strain rates. Similar strain rates have been used to study the mechanical properties of PGNs through CG-MD simulations.[27,49]

C. Chain length and size effects

The parameter space of PGNs can be decomposed into the grafted chain length and nanoparticle core radius (Fig. 4) to analyze their effects on the shear modulus (G). Figure 4(a) shows G as a function of polymer chain length for linear chains and PGNs of nanoparticle radii 5 and 8 (σ). The full set of PGN systems are presented in the supplementary material (Fig. S5); however, the trends are well represented with the presented reduced plot. It should be noted that a nanoparticle radius of 0 (σ) represents the linear polymer system with no nanoparticles. Focusing on the behavior of the linear chains, an expected rough constant G is observed for all chain lengths. For the lowest chain length (N = 20), a decrease in G is expected due to the chain being shorter than the determined entanglement length of the polymer model ($N_e \approx 35$).[22,31,32] More interestingly, PGN systems with lower chain lengths are found to result in higher measured G. As the grafted chain length increases for these systems, G decreases to converge to roughly the same G as that of linear ungrafted polymer chain systems. The behavior of this relationship is attributed to long grafted chain lengths resulting in lower nanoparticle volume fractions, which are analyzed in greater depth in the proceeding volume fraction analysis and the conformation analysis. An increase in elastic modulus with decreasing chain

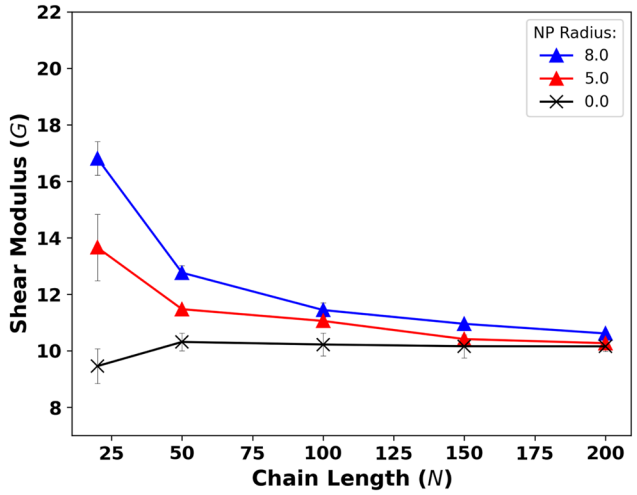

(a)

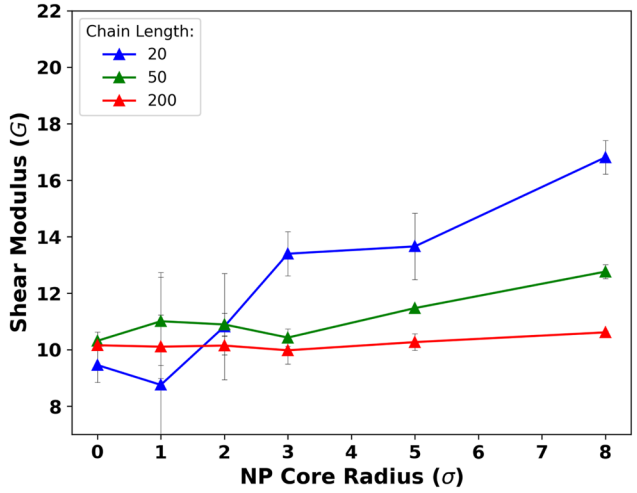

(b)

FIG. 4. Effects of (a) chain length and (b) nanoparticle core size on G at a constant shear rate [$\dot{\gamma} = 10^{-5}$ (τ^{-1})].

length was reported in the previous work for star polymers with higher than 12 arms. Consequently, this implies a possible increase in the nanoconfinement of the polymer chains and a higher fraction of polymers existing in a concentrated brush regime.[62]

Figure 4(b) shows G as a function of nanoparticle core radius for chain lengths of 20, 50, and 200 (N) for clarity. The complete set of chain lengths is provided in the supplementary material (Fig. S6). As expected from the chain length effects, the short chain length systems are more strongly affected by the variance of nanoparticle radius. In general, as the nanoparticle core radius increases, the observed G increases. However, for large chain lengths, more specifically $N = 200$, G remains roughly unaffected by the increased nanoparticle radius. The slight non-monotonic behavior of G with increasing nanoparticle radius, primarily at low nanoparticle radii, is expected to be statistically insignificant. The error reported for low nanoparticle radius systems is high relative to larger radius systems. This elevated error is primarily attributed to the varied system packing structures for small nanoparticle radii post-equilibration. The equilibrated structure assemblies subjected to shear deformation exhibit greater dissimilarity in small nanoparticle radii systems, contrasting with the fairly uniform equilibrated structures observed in systems with larger nanoparticle radii. As mentioned in Sec. II C, *System Equilibration*, systems with larger nanoparticle radii tend to stay close to their FCC packing structure throughout the equilibration, while small nanoparticle radii systems shift to a disordered arrangement due to the decrease in available void space for relaxed polymer chain segments.

The trends shown in Fig. 4(b) point to a material stiffening effect due to the higher volume of rigid nanoparticles throughout the system. As the bulk material transitions to higher portions of softer polymeric make-up, the total response tends to that of the majority material's behavior, which would be a softer and reduced G. Overall, the coupling effect of the chain length and nanoparticle core radius shown in Fig. 4 leads to the notion that the shear response of PGNs can culminate into a volume fraction argument, which is discussed in further detail below.

D. Conformation analysis

To further understand what factors may affect the shear response mechanics for different polymer-grafted nanoparticle systems, the monomer radial positions of the grafted chains are analyzed. Figure 5 shows the plots of the average radial distance of monomers along the polymer chain vs the index of monomers starting from the grafted site on the nanoparticle surface. Near the surface of nanoparticles, "concentrated polymer brush" (CPB) regions are expected to form, creating a stiff shell of stretched polymer chains. Further out from the nanoparticle surface, a "semidilute polymer brush" (SDPB) region is expected, where chain conformations are more relaxed. A common practice throughout the literature is to fit a linear relationship between low-index monomers as the CPB region, in which the radial distance of polymer chains is expected to scale as $R \sim N$. Between high index monomers in the SDPB region, the radial distance of polymer chains is expected to transition to scale as $R \sim \sqrt{N}$.[10,15] Figure 5 additionally shows these expected scaling behaviors as a reference. The coefficients used for the expected theoretical behavior are estimated by incrementally fitting the monomer position indices beginning from the last index, which is expected to match the form $R_i \sim N^{0.5}$. Generally, the first few monomers appear to follow the expected scaling of the CPB region, and the remaining chain transitions close to the expected scaling of the SDPB region. The lack of strong visual correlation to a linear region may be due to the necessary conditions of short chains highly grafted onto low curvature surfaces.[7] An equation defining the crossover radius as the point at which a transition from the CPB to SDPB regime will occur is given by Ohno *et al.*[10] The equation leads to the expectation that the crossover radius will increase as the nanoparticle core radius increases. This relationship is consistent with the results regarding the conformations of spherical polymer brushes of past studies.[7,63] Evaluating the exact point of this transition is not within the scope of this research and is, therefore, not quantified. However, this question does warrant future investigation on further quantifying the transitional point for similar PGN

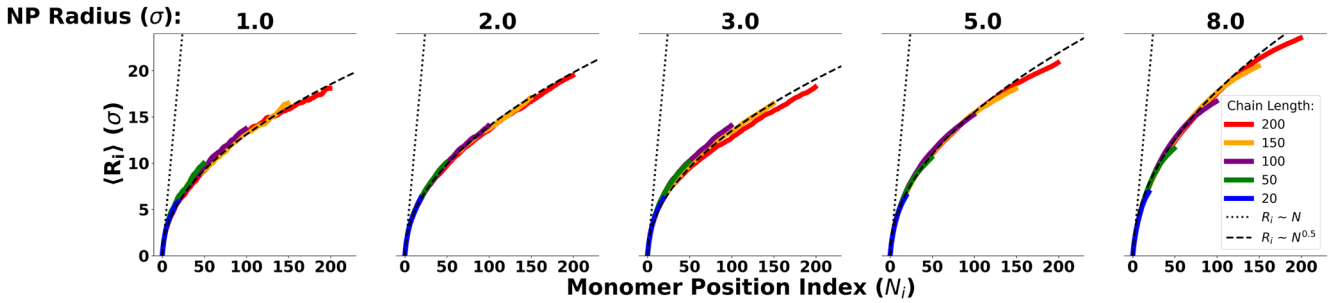

FIG. 5. Radial distance of monomers from the surface of the nanoparticle.

systems. Notably, the theoretically expected scaling of the SDPB region reveals that large nanoparticle systems experience curling of the grafted polymer free ends. Specifically, for nanoparticle radii of 5 and 8 (σ) and more pronounced for long chains, the free ends are found to scale roughly as $R \sim N^{1/3}$. This is indicative of a poor solvent condition[64] for the interstitial regions of these PGN systems. This effect is likely due to an increase in the available interstitial void space and restriction from the surrounding dense polymer coronas.

Snapshots taken of simulated system trajectories[65] are shown in Fig. 6 to aid in the physical visualization of this confining effect. The deep red highlighted beads belong to a single selected PGN, including its nanoparticle beads and grafted polymer chain beads. All other beads are rendered with transparency to provide a three-dimensional view of the simulation box. White transparent beads are grafted polymer chains, and the faint dark circles are other nanoparticles. Large nanoparticle radii systems are expected to offer greater available void space in the interstitial zones, allowing polymer free ends to reside in close proximity to their nanoparticle.[58] Additionally, neighboring dense coronas likely confine these free polymer ends to remain in their immediate interstitial regions. Figure 6(a) shows the equilibrated PGN system of the nanoparticle radius of 8 (σ) and chain length of 200 (N). In this image, the grafted polymer chain free ends of the selected PGN do not reach far out in the space of the simulation box but are restricted to the interstitial pockets around their nanoparticle. This restriction likely contributes to the curling of the free polymer ends of large nanoparticle radii systems. Contrarily, small nanoparticle radii are expected to offer lower available void space between PGNs, which may force free polymer chain ends outside of their close interstitial regions and allow them to be more relaxed/stretched. Figure 6(b) shows the equilibrated PGN system of nanoparticle radius of 3 (σ) and chain length of 200 (N). The grafted polymer chain free ends of the selected PGN in this system reach relatively far out into the space of the simulation box. Some polymer free ends appear to extend significantly, exploring interstitial pockets of neighboring PGNs. This extension allows for the more relaxed state of polymer free ends in comparison to the confined free ends in the large nanoparticle radius systems. Figure 6(c) supplements these observations by showing the probability distribution of the end-to-end distance (R_{ee}) of each grafted polymer chain of length 200 (N) normalized by their respective average NP–NP spacing (d_{NP}). The probability distributions are for systems with nanoparticles of radii 3 and 8 (σ). For nanoparticles of radii 3 (σ), the mode of the skewed distribution, shows that most chains are extended to roughly the distance of their NP–NP spacing. However, the average end-to-end distance appears to be greater than that of their NP–NP spacing, indicating that the ends of many chains reach far into the interstitial pockets of neighboring PGNs. The relatively normal distribution for nanoparticles of radii 8 (σ) shows that the NP–NP spacing exceeds the average end-to-end distance of their grafted polymer chains. This confirms that most free ends of their grafted chains are restricted to the immediate interstitial pockets surrounding their nanoparticle.

Additionally, the average end-to-end distance of the grafted polymer chains is plotted as a function of nanoparticle core radius for each system shown in Fig. 7. The roughly constant behavior of the end-to-end distance for each chain length is presumably due to their constant grafted density, resulting in the formation of a dense polymer corona. The high grafting density of the polymer corona prohibits grafted chains from forming "mushroom" configurations on the surface of nanoparticles with low end-to-end distances.[66] There is an observed increase in end-to-end distance as the nanoparticle core radius is increased. The increase in radius leading to the flattening of the nanoparticle surface likely induces overcrowding effects near the grafting points at the nanoparticle surface. Higher confinement forces a greater extension of the polymer in this region due to the decreased available space between chains. This is in line with the previous theory regarding the effect of the curvature of the grafting surface on polymer chain conformations.[7,63] As the curvature of the surface diminishes (with an increase in nanoparticle radius), the transition from a confined brush region to relaxed chains occurs at longer chain lengths, resulting in an extension of the end-to-end distance.

The Debye–Waller factor (DWF) is also considered for fast chain dynamical analysis.[67] The factor is measured as the average monomer mean square displacement ($\langle u^2 \rangle$) within its caging region.[68] In this work, $\langle u^2 \rangle$ is referred to as the DWF following the methods of previous simulation studies.[68,69] The time a monomer spends in its caging region, the caging time, is taken as 1 (τ) of the simulation in the equilibrium state for each PGN system, aligning with the caging time used by the previous work calculating the DWF for CGMD simulations.[70] Figure 8 shows the DWF as a function of the monomer index of the nanoparticle of radius 2 and 8 (σ) PGN systems for clarity in the conformation explanation; the complete parameter space is shown in Fig. S7 of the supplementary material. For the average $\langle u^2 \rangle$ over all monomers for the system

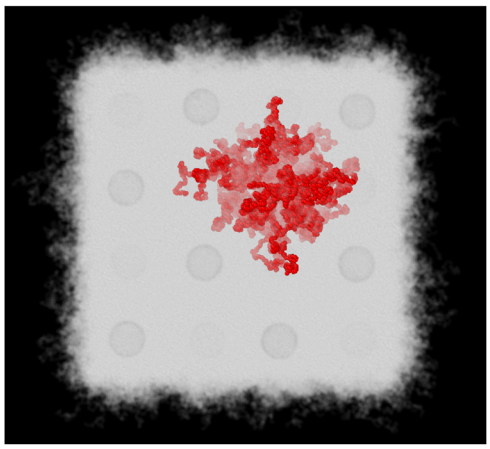

(a)

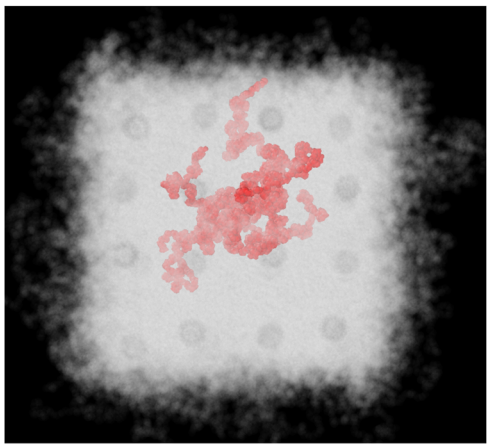

(b)

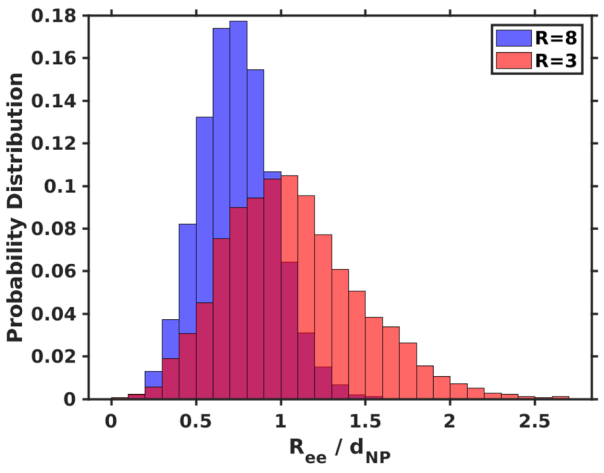

(c)

FIG. 6. Snapshots of system trajectories post-equilibration for PGNs with nanoparticle radii and grafted chain lengths of (a) 8 (σ) and 200 (N) and (b) 3 (σ) and 200 (N), respectively, and (c) probability distribution of end-to-end distances normalized by the respective average NP–NP spacing for systems with nanoparticle radii of 3 and 8 (σ).

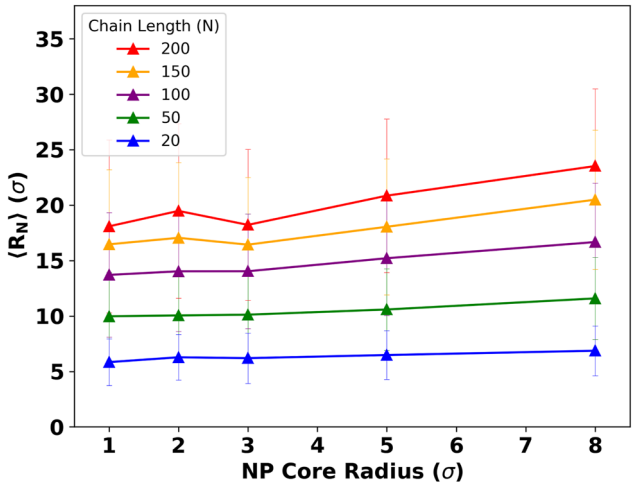

FIG. 7. End-to-end distance of grafted polymer chains ($\langle R_N \rangle$) as a function of nanoparticle core radius.

containing nanoparticles with a radius of 8, the DWF can be taken as roughly 0.032 (σ^2). Prior studies quantifying the DWF for similar KG polymer systems find that $\langle u^2 \rangle$ for systems slightly below their glass transition temperature also fall in the vicinity of 0.03 (σ^2).[70]

This study uses $\langle u^2 \rangle$ to analyze the segmental mobility of the polymer chains grafted to the surface of the nanoparticle. Three distinct regions are observed in the analysis of the DWF: an initial increase, a plateau, and a final increase. The initial increase with a low magnitude of $\langle u^2 \rangle$ is found to correlate to the first few monomers of the grafted polymer chains, close to the surface of the nanoparticle. At the surface of the nanoparticle, chains are heavily confined due to the grafted-chain density causing a caged dynamic motion. However, as the plateau region is reached, for the majority of the polymer chain length, the monomers are seen to be in a semi-mobile state in comparison to low-index monomers. The monomers in this plateau are confined to local motion but still restricted by neighboring chains. Finally, in the last few monomers of each chain length, an additional increase is observed correlating to the free ends of the grafted polymer chains. The free ends are allowed to explore different conformations with much less cage restriction. The analysis presents a physical picture to explain the nanoparticle-to-nanoparticle interactions. Close to the surface of the nanoparticle, a hard shell region of confined polymer chains is observed, and further away, a softer shell comprised of polymer chain free ends allows intermingling with the coronas of nearby PGNs. Although grafted chain density is held as a constant throughout all systems, for smaller nanoparticles, less distinction can be made between the three regions of mobility. The heavy noise in smaller nanoparticle systems is attributed to the fewer total chains averaged compared to large nanoparticle systems. The region transitions show the chains of small grafted nanoparticles to be less confined and, therefore, more likely to interpenetrate the full corona of neighboring PGNs. In contrast, greater confinement effects in larger nanoparticle systems provide additional stiffening behavior at the surface of the nanoparticles acting as an effective stiff core. Furthermore, the distinct softer

region of polymer free ends may more easily interpenetrate only the soft regions of other PGNs. These pronounced distinctions in caged polymer dynamics likely contribute to the enhanced shear modulus found in large nanoparticle systems.

E. Volume fraction effect

The prominent effects of the nanoparticle size in competition with the effects of chain length in grafted vs ungrafted chains lead to the conclusion that volume fraction effects of nanoparticles on the polymer are dominant in the determination of G. To better understand this conclusion in the behavior of the PGN systems, G is plotted as a function of the volume fraction of nanoparticles (Fig. 9). Only plots with a selected few shear rates are provided here; however, the full parameter space is provided in the supplementary material (Fig. S8). This volume fraction is calculated by taking the ratio of the sum of nanoparticle volumes (Vol_{NP}) to the total simulation box volume (Vol_{box}) [Eq. (3)],

$$\Phi_{NP} = \frac{\sum_{n=1}^{32} Vol_{NP}}{Vol_{box}}. \tag{3}$$

For statistical accuracy, these results are taken as an average over three trials, and the standard deviation is displayed. Analyzing 0.00 Φ_{NP} provides the G for linear polymer chains (no nanoparticles). In this comparison, throughout all evaluated shear rates, G for linear polymer chains remains relatively constant, only showing fluctuation as a function of shear rate. At a high shear rate [Fig. 9(a)], the G values for different systems are clustered, showing no distinct trend. This ambiguity is attributed to the elevated error of the high shear strain rates previously stated in the strain rate dependency analysis. However, it is interesting to analyze points near similar volume fractions, achievable by the variations in polymer length as well as nanoparticle size, resulting in more polymer beads due to constant grafted density. At similar volume fractions where data points cluster, for example, $\Phi_{NP} \approx 0.02$, the small radius PGN system (1 σ) appears to hold higher G values than the nearby larger radius systems 2, 3, and 5 (σ). Additionally, the relatively elevated G of small nanoparticle radii hold lower grafted chain lengths than those of the larger nanoparticles near the same Φ_{NP}. The intricate influence of the nanoparticle size and chain length is expected to be secondary to the effects of Φ_{NP} on the measurement of G. This observation is consistent with the analyzed effects of chain length for PGN materials exhibiting similar monotonically increasing shear modulus with increasing nanoparticle filling fractions.[71] The results of the previous study indicate that the shear modulus of PGNs depends on the chain length and grafted density of systems with approximately equal nanoparticle filling fractions. However, the influence of the nanoparticle size and chain length is expected to be secondary to the effects of Φ_{NP}, which holds a more prominent linear correlation to the measurement of G.

At shear rates below 0.01 (τ^{-1}), a recognizable trend emerges. The data are well-fitted to an adapted formulation of a general rule of mixtures, provided by the Voigt modulus,[72] displayed in the following equation:

$$G_{PGN} = \Phi_{NP} \cdot G_{NP} + (1 - \Phi_{NP}) \cdot G_{linear}, \tag{4}$$

where G_{PGN} is the shear modulus of the PGN system, Φ_{NP} is the volume fraction of nanoparticles in the PGN system, and G_{linear} is the shear modulus of the pure linear chain system. This formulation assumes an equivalent strain within the composite's reinforcement (nanoparticles) and matrix (polymers) as well as a linear-elastic material response. Equation (4) is fitted to the corresponding data shown in Fig. 9 by employing non-linear least squares optimization to tune the parameters of G_{NP} and G_{linear}. The fits are shown in Fig. 9, indicated by the black dotted line, and the respective parameters are provided in Table I. At a vanishing value of Φ_{NP}, G_{PGN} holds no dependence on G_{NP}, indicating that the contribution to G_{PGN} resorts entirely to G of the linear polymer chain system. The fitted G_{linear} values are approximately equal to the arithmetic mean of the linear chain values of G. Conversely, the maximized value of $\Phi_{NP} = 1$ indicates G_{PGN} with the sole contribution from G_{NP} and no dependence on G_{linear}. While this model accurately captures the behavior of low Φ_{NP} systems, caution must be exercised in the extrapolation

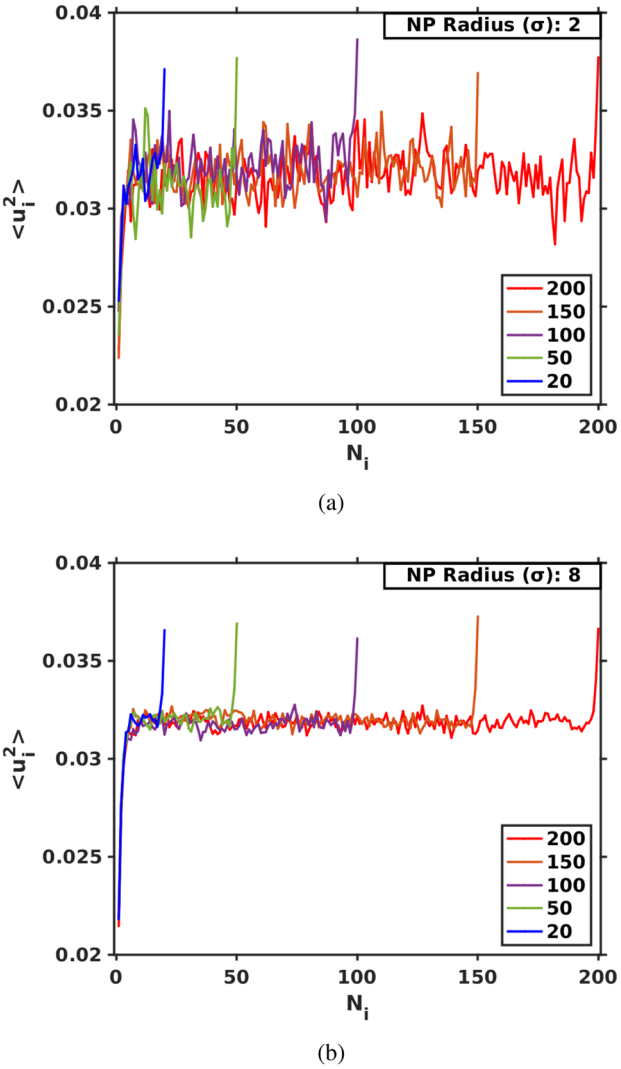

FIG. 8. Debye–Waller factor of the PGN system with nanoparticle radii of (a) 2 and (b) 8 (σ).

TABLE I. G_{NP} and G_{linear} for varying shear rates.

Shear rate ($\dot{\gamma}$)	G_{NP} (p^*)	G_{linear} (p^*)
0.000 01	40.42	9.84
0.000 05	42.78	10.75
0.000 1	44.93	11.13
0.000 5	48.23	12.06
0.001	47.32	12.29
0.005	43.38	12.82
0.01	32.37	12.58

of the value of G_{NP}. The NP–NP interactions are not considered in this work as they are negligible given the steric hindrances of grafted polymers, but this does not hold true for bare particles. Therefore, a parameterized model of a purely nanoparticle system to capture this data point is not within the scope of this research.

Most prominently, as shown in Figs. 9(b)–9(d), G appears to collapse to a more discernible linear correlation with the volume fraction of nanoparticles present within the system. The difference in the trend of high shear rate simulation (0.01 τ^{-1}) [Fig. 9(a)] is attributed to the increased error described in the shear rate effects. As the volume fraction of nanoparticles increases, the measured G increases. This is an expected observation given that nanoparticles are typically much more rigid than polymeric materials. As a system is filled with a more rigid material, the total material property tends to align with that of the introduced material; in this case, rigid nanoparticles.

The relationship between Φ_{NP} and G displayed in this study is supplemented by the findings of Jhalaria *et al.*,[73] where the shear modulus (G) was studied for poly(methyl acrylate) (PMA) grafted silica nanoparticles. In consensus with this research, their findings show shear modulus enhancement as a function of increasing nanoparticle volume fraction. While they observe a slightly nonlinear behavior, the qualitative increase is verified. From Eq. (4), G_{NP} and G_{linear} of Jhalaria *et al.* are estimated to be 18.78 and 7.32 GPa, respectively. Due to the lack of a distinct trend within the values of G_{NP} and G_{linear} of this study, the arithmetic mean of the data [G_{NP} = 42.78 (p^*) and G_{linear} = 11.65 (p^*)] are taken to compare with the findings of Jhalaria *et al.* The ratio of G_{linear} GPa of Jhalaria *et al.* to the average G_{linear} (p^*) of this study can be used as a scalar value (α) for mapping Eq. (4). The value of α is determined to be roughly 0.645 GPa/p^*. The maximum of G_{NP} of this study multiplied by α yields G_{NP} = 27.59 GPa, which is greater than the value presented by Jhalaria *et al.* (18.78 GPa). It is noted that the work of Jhalaria *et al.* was conducted above the glass transition of their grafted polymer chains. Additionally, their findings are high-frequency measurements in which the high rate may have an effect on the trend as well as magnitude of G. Although the qualitative behavior of the findings is in agreement, the difference in the quantitative analysis is expected to be a result of the nanoparticle interactions considered in this study as well as the different grafted chain densities and specific polymer chemistry in the findings of Jhalaria *et al.*. The effects of these parameters are not specifically addressed within the scope of this research. However, these findings warrant future investigation to resolve the dependence of the value of G on additional parameters of interest, such as grafted density and grafted polymer chemistry.

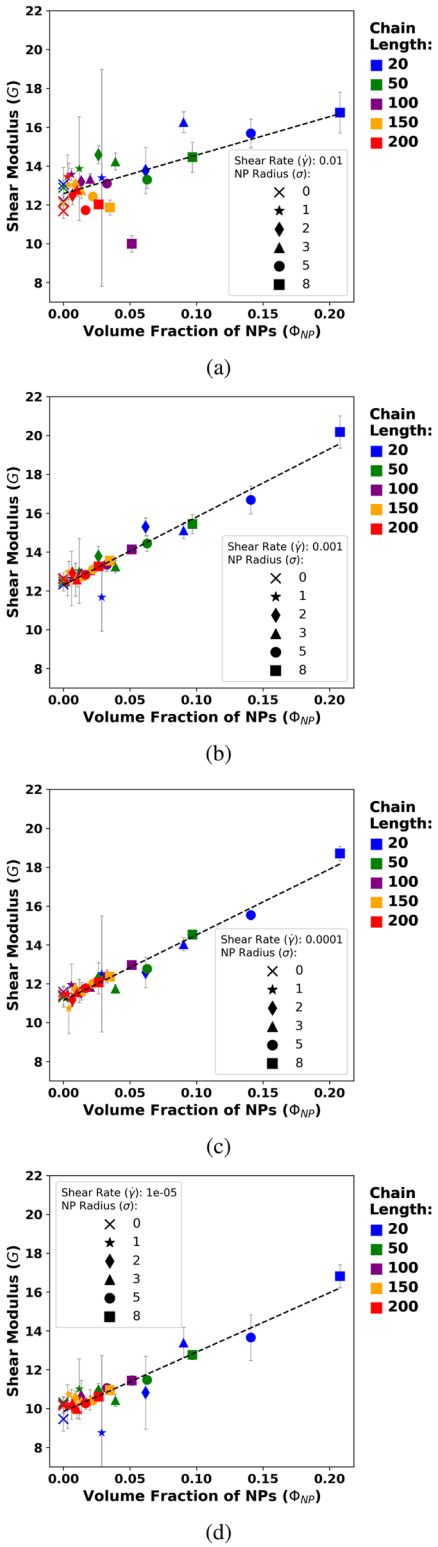

FIG. 9. Shear modulus (G) as a function of volume fraction of nanoparticles at (a) 0.01, (b) 0.001, (c) 0.0001, and (d) and 0.000 01 (τ^{-1}).

IV. CONCLUSION

This study characterizes the shear mechanical response of polymer grafted nanoparticles (PGNs) by obtaining the shear modulus (G) through molecular dynamics simulations. The shear rate of deformation influences the response of the systems by increasing G as the rate is increased. This trend is seen to decompose at large shear rates, justified by the relatively high corresponding error of these points due to heightened simulation noise. As the grafted polymer chain length decreases, G increases due to effective stiffening, which is seen through a conformational analysis. The dynamics of chain conformations reveal distinct regions of caged monomer motion in larger nanoparticle systems, which also contributes to the enhanced values of G. Chain conformations of large nanoparticle systems reveal poor solvent conditions in the interstitial pockets of the PGNs. This phenomenon is expected to be a result of the availability of free volume in these regions, stemming from a reduction in nanoparticle surface curvature. The curvature of the nanoparticle surface introduces additional confining effects, leading to the elongation of the end-to-end distances most prominently in long polymer chains. The size of the nanoparticle displays an expected effect of increased G for larger nanoparticles. The reason for this relationship again primarily stems from the increase in the volume fraction of nanoparticles. To further understand the relationship between the volume fractions of nanoparticles and shear modulus, a simple rule of mixtures formulation is used to model G as a function of Φ_{NP}. The qualitative analysis of this trend is verified by recent experimental work. However, quantitative disparities warrant a continued investigation into systems approaching the upper bounds of Φ_{NP}. Furthermore, the parameters not addressed in this study, such as grafted density and polymer chemistry, require further examination into their effects on G. The insights provided by this research add to the ongoing development of PGN simulations for future studies. The simulations and results presented here advocate for the expansion of comprehensive models that capture intricate details from shear mechanical properties to tensile strength and toughness characterization of prior research findings. In conclusion, the thorough parametric study conducted in this research not only contributes to advances in understanding the shear mechanical properties of PGNs below their glass transition temperature but also paves the way for new insights into the intricate attributes of the PGN material response.

SUPPLEMENTARY MATERIAL

See the supplementary material for the detailed analyses referenced in the main text.

ACKNOWLEDGMENTS

This work was supported by the Army Research Office (Grant No. W911NF2210287) and the National Science Foundation (Grant No. DMR-2308691). Access to a supercomputing grant from the Quest High-Performance-Computing System at the Northwestern University is also acknowledged. S.P. acknowledges the support from the International Institute for Nanotechnology at the Northwestern University.

AUTHOR DECLARATIONS

Conflict of Interest

The authors have no conflicts to disclose.

Author Contributions

Arman Moussavi: Conceptualization (lead); Data curation (lead); Formal analysis (lead); Investigation (lead); Methodology (lead); Validation (lead); Visualization (lead); Writing – original draft (lead); Writing – review & editing (equal). **Subhadeep Pal**: Formal analysis (supporting); Investigation (supporting); Writing – review & editing (supporting). **Zhenghao Wu**: Conceptualization (supporting); Formal analysis (supporting); Supervision (supporting); Writing – review & editing (supporting). **Sinan Keten**: Formal analysis (equal); Funding acquisition (lead); Investigation (equal); Project administration (lead); Resources (lead); Supervision (lead); Writing – review & editing (equal).

DATA AVAILABILITY

The data that support the findings of this study are available from the corresponding author upon reasonable request.

REFERENCES

[1] M. J. Hore, L. T. Korley, and S. K. Kumar, "Polymer-grafted nanoparticles," J. Appl. Phys. **128**, 030401 (2020).
[2] S. K. Kumar, B. C. Benicewicz, R. A. Vaia, and K. I. Winey, "50th anniversary perspective: Are polymer nanocomposites practical for applications?," Macromolecules **50**, 714–731 (2017).
[3] S. K. Kumar, N. Jouault, B. Benicewicz, and T. Neely, "Nanocomposites with polymer grafted nanoparticles," Macromolecules **46**, 3199–3214 (2013).
[4] S. K. Kumar and R. Krishnamoorti, "Nanocomposites: Structure, phase behavior, and properties," Annu. Rev. Chem. Biomol. Eng. **1**, 37–58 (2010).
[5] A. C. Balazs, T. Emrick, and T. P. Russell, "Nanoparticle polymer composites: Where two small worlds meet," Science **314**, 1107–1110 (2006).
[6] Z. Wu, S. Pal, and S. Keten, "Implicit chain particle model for polymer-grafted nanoparticles," Macromolecules **56**, 3259–3271 (2023).
[7] D. Dukes, Y. Li, S. Lewis, B. Benicewicz, L. Schadler, and S. K. Kumar, "Conformational transitions of spherical polymer brushes: Synthesis, characterization, and theory," Macromolecules **43**, 1564–1570 (2010).
[8] N. J. Fernandes, H. Koerner, E. P. Giannelis, and R. A. Vaia, "Hairy nanoparticle assemblies as one-component functional polymer nanocomposites: Opportunities and challenges," MRS Commun. **3**, 13–29 (2013).
[9] W. R. Lenart and M. J. Hore, "Structure–property relationships of polymer-grafted nanospheres for designing advanced nanocomposites," Nano-Struct. Nano-Objects **16**, 428–440 (2018).
[10] K. Ohno, T. Morinaga, S. Takeno, Y. Tsujii, and T. Fukuda, "Suspensions of silica particles grafted with concentrated polymer brush: Effects of graft chain length on brush layer thickness and colloidal crystallization," Macromolecules **40**, 9143–9150 (2007).
[11] J. Midya, M. Rubinstein, S. K. Kumar, and A. Nikoubashman, "Structure of polymer-grafted nanoparticle melts," ACS Nano **14**, 15505–15516 (2020).
[12] N. K. Hansoge, A. Gupta, H. White, A. Giuntoli, and S. Keten, "Universal relation for effective interaction between polymer-grafted nanoparticles," Macromolecules **54**, 3052–3064 (2021).
[13] N. K. Hansoge and S. Keten, "Effect of polymer chemistry on chain conformations in hairy nanoparticle assemblies," ACS Macro Lett. **8**, 1209–1215 (2019).
[14] F. Müller-Plathe, "Coarse-graining in polymer simulation: From the atomistic to the mesoscopic scale and back," ChemPhysChem **3**, 754–769 (2002).

[15]N. K. Hansoge, T. Huang, R. Sinko, W. Xia, W. Chen, and S. Keten, "Materials by design for stiff and tough hairy nanoparticle assemblies," ACS Nano **12**, 7946–7958 (2018).
[16]J. G. Ethier and L. M. Hall, "Structure and entanglement network of model polymer-grafted nanoparticle monolayers," Macromolecules **51**, 9878–9889 (2018).
[17]J. G. Ethier, L. F. Drummy, R. A. Vaia, and L. M. Hall, "Uniaxial deformation and crazing in glassy polymer-grafted nanoparticle ultrathin films," ACS Nano **13**, 12816–12829 (2019).
[18]P. Akcora, H. Liu, S. K. Kumar, J. Moll, Y. Li, B. C. Benicewicz, L. S. Schadler, D. Acehan, A. Z. Panagiotopoulos, V. Pryamitsyn *et al.*, "Anisotropic self-assembly of spherical polymer-grafted nanoparticles," Nat. Mater. **8**, 354–359 (2009).
[19]T. Lafitte, S. K. Kumar, and A. Z. Panagiotopoulos, "Self-assembly of polymer-grafted nanoparticles in thin films," Soft Matter **10**, 786–794 (2014).
[20]G. D. Hattemer and G. Arya, "Viscoelastic properties of polymer-grafted nanoparticle composites from molecular dynamics simulations," Macromolecules **48**, 1240–1255 (2015).
[21]T.-Y. Tang and G. Arya, "Anisotropic three-particle interactions between spherical polymer-grafted nanoparticles in a polymer matrix," Macromolecules **50**, 1167–1183 (2017).
[22]K. Kremer and G. S. Grest, "Dynamics of entangled linear polymer melts: A molecular-dynamics simulation," J. Chem. Phys. **92**, 5057–5086 (1990).
[23]H. Chao and R. A. Riggleman, "Effect of particle size and grafting density on the mechanical properties of polymer nanocomposites," Polymer **54**, 5222–5229 (2013).
[24]M. Giovino, J. Pribyl, B. Benicewicz, S. Kumar, and L. Schadler, "Linear rheology of polymer nanocomposites with polymer-grafted nanoparticles," Polymer **131**, 104–110 (2017).
[25]C. Chevigny, F. Dalmas, E. Di Cola, D. Gigmes, D. Bertin, F. Boué, and J. Jestin, "Polymer-grafted-nanoparticles nanocomposites: Dispersion, grafted chain conformation, and rheological behavior," Macromolecules **44**, 122–133 (2011).
[26]J. F. Moll, P. Akcora, A. Rungta, S. Gong, R. H. Colby, B. C. Benicewicz, and S. K. Kumar, "Mechanical reinforcement in polymer melts filled with polymer grafted nanoparticles," Macromolecules **44**, 7473–7477 (2011).
[27]H. Li, R. Ma, W. Zhang, S. Hu, X. Zhao, L. Zhang, and Y. Gao, "Stress overshoot behavior in polymer nanocomposites filled with spherical nanoparticles under steady shear flow via molecular dynamics simulation," Mater. Today Commun. **35**, 105573 (2023).
[28]D. Maillard, S. K. Kumar, B. Fragneaud, J. W. Kysar, A. Rungta, B. C. Benicewicz, H. Deng, L. C. Brinson, and J. F. Douglas, "Mechanical properties of thin glassy polymer films filled with spherical polymer-grafted nanoparticles," Nano Lett. **12**, 3909–3914 (2012).
[29]A. P. Thompson, H. M. Aktulga, R. Berger, D. S. Bolintineanu, W. M. Brown, P. S. Crozier, P. J. in't Veld, A. Kohlmeyer, S. G. Moore, T. D. Nguyen, R. Shan, M. J. Stevens, J. Tranchida, C. Trott, and S. J. Plimpton, "LAMMPS - A flexible simulation tool for particle-based materials modeling at the atomic, meso, and continuum scales," Comput. Phys. Commun. **271**, 108171 (2022).
[30]G. S. Grest and K. Kremer, "Molecular dynamics simulation for polymers in the presence of a heat bath," Phys. Rev. A **33**, 3628 (1986).
[31]G. S. Grest, M. Pütz, R. Everaers, and K. Kremer, "Stress–strain relation of entangled polymer networks," J. Non-Cryst. Solids **274**, 139–146 (2000).
[32]E. R. Duering, K. Kremer, and G. S. Grest, "Dynamics of model networks: The role of the melt entanglement length," Macromolecules **26**, 3241–3244 (1993).
[33]V. Goel, J. Pietrasik, H. Dong, J. Sharma, K. Matyjaszewski, and R. Krishnamoorti, "Structure of polymer tethered highly grafted nanoparticles," Macromolecules **44**, 8129–8135 (2011).
[34]V. V. Ginzburg, "Modeling the morphology and phase behavior of one-component polymer-grafted nanoparticle systems," Macromolecules **50**, 9445–9455 (2017).
[35]H. Yun, J. W. Yu, Y. J. Lee, J.-S. Kim, C. H. Park, C. Nam, J. Han, T.-Y. Heo, S.-H. Choi, D. C. Lee *et al.*, "Symmetry transitions of polymer-grafted nanoparticles: Grafting density effect," Chem. Mater. **31**, 5264–5273 (2019).
[36]H. Zhang, W. Wang, M. Akinc, S. Mallapragada, A. Travesset, and D. Vaknin, "Assembling and ordering polymer-grafted nanoparticles in three dimensions," Nanoscale **9**, 8710–8715 (2017).
[37]Y. N. Pandey, G. J. Papakonstantopoulos, and M. Doxastakis, "Polymer/nanoparticle interactions: Bridging the gap," Macromolecules **46**, 5097–5106 (2013).
[38]Y. Zhu, A. Giuntoli, W. Zhang, Z. Lin, S. Keten, F. W. Starr, and J. F. Douglas, "The effect of nanoparticle softness on the interfacial dynamics of a model polymer nanocomposite," J. Chem. Phys. **157**, 094901 (2022).
[39]M. J. Hamer, B. V. Iyer, V. V. Yashin, T. Kowalewski, K. Matyjaszewski, and A. C. Balazs, "Modeling polymer grafted nanoparticle networks reinforced by high-strength chains," Soft Matter **10**, 1374–1383 (2014).
[40]H. Kamberaj, R. Low, and M. Neal, "Time reversible and symplectic integrators for molecular dynamics simulations of rigid molecules," J. Chem. Phys. **122**, 224114 (2005).
[41]S. K. Sukumaran, G. S. Grest, K. Kremer, and R. Everaers, "Identifying the primitive path mesh in entangled polymer liquids," J. Polym. Sci., Part B: Polym. Phys. **43**, 917–933 (2005).
[42]T. Vettorel and K. Kremer, "Development of entanglements in a fully disentangled polymer melt," Macromol. Theory Simul. **19**, 44–56 (2010).
[43]W. B. Lee and K. Kremer, "Entangled polymer melts: Relation between plateau modulus and stress autocorrelation function," Macromolecules **42**, 6270–6276 (2009).
[44]R. S. Hoy and G. S. Grest, "Entanglements of an end-grafted polymer brush in a polymeric matrix," Macromolecules **40**, 8389–8395 (2007).
[45]N. C. Karayiannis, V. G. Mavrantzas, and D. N. Theodorou, "A novel Monte Carlo scheme for the rapid equilibration of atomistic model polymer systems of precisely defined molecular architecture," Phys. Rev. Lett. **88**, 105503 (2002).
[46]S. W. Sides, G. S. Grest, M. J. Stevens, and S. J. Plimpton, "Effect of end-tethered polymers on surface adhesion of glassy polymers," J. Polym. Sci., Part B: Polym. Phys. **42**, 199–208 (2004).
[47]R. Auhl, R. Everaers, G. S. Grest, K. Kremer, and S. J. Plimpton, "Equilibration of long chain polymer melts in computer simulations," J. Chem. Phys. **119**, 12718–12728 (2003).
[48]W. Tao, J. Shen, Y. Chen, J. Liu, Y. Gao, Y. Wu, L. Zhang, and M. Tsige, "Strain rate and temperature dependence of the mechanical properties of polymers: A universal time-temperature superposition principle," J. Chem. Phys. **149**, 044105 (2018).
[49]J. Wang and T. Ge, "Crazing reveals an entanglement network in glassy ring polymers," Macromolecules **54**, 7500–7511 (2021).
[50]J. Rottler and M. O. Robbins, "Growth, microstructure, and failure of crazes in glassy polymers," Phys. Rev. E **68**, 011801 (2003).
[51]D. Meng, S. K. Kumar, T. Ge, M. O. Robbins, and G. S. Grest, "Crazing of nanocomposites with polymer-tethered nanoparticles," J. Chem. Phys. **145**, 094902 (2016).
[52]M. J. Stevens, "Manipulating connectivity to control fracture in network polymer adhesives," Macromolecules **34**, 1411–1415 (2001).
[53]T. Ge, M. O. Robbins, D. Perahia, and G. S. Grest, "Healing of polymer interfaces: Interfacial dynamics, entanglements, and strength," Phys. Rev. E **90**, 012602 (2014).
[54]T. Ge, G. S. Grest, and M. O. Robbins, "Tensile fracture of welded polymer interfaces: Miscibility, entanglements, and crazing," Macromolecules **47**, 6982–6989 (2014).
[55]T. Ge, G. S. Grest, and M. O. Robbins, "Structure and strength at immiscible polymer interfaces," ACS Macro Lett. **2**, 882–886 (2013).
[56]T. Ge, F. Pierce, D. Perahia, G. S. Grest, and M. O. Robbins, "Molecular dynamics simulations of polymer welding: Strength from interfacial entanglements," Phys. Rev. Lett. **110**, 098301 (2013).
[57]M. J. Stevens, "Interfacial fracture between highly cross-linked polymer networks and a solid surface: Effect of interfacial bond density," Macromolecules **34**, 2710–2718 (2001).
[58]J. Choi, C. M. Hui, M. Schmitt, J. Pietrasik, S. Margel, K. Matyjazsewski, and M. R. Bockstaller, "Effect of polymer-graft modification on the order formation in particle assembly structures," Langmuir **29**, 6452–6459 (2013).
[59]P. J. Daivis and B. Todd, "A simple, direct derivation and proof of the validity of the SLLOD equations of motion for generalized homogeneous flows," J. Chem. Phys. **124**, 194103 (2006).

[60]A. Giuntoli, N. K. Hansoge, A. van Beek, Z. Meng, W. Chen, and S. Keten, "Systematic coarse-graining of epoxy resins with machine learning-informed energy renormalization," npj Comput. Mater. **7**, 168 (2021).
[61]U. Gurel and A. Giuntoli, "Shear thinning from bond orientation in model unentangled bottlebrush polymer melts," Macromolecules **56**, 5708–5717 (2023).
[62]A. Giuntoli and S. Keten, "Tuning star architecture to control mechanical properties and impact resistance of polymer thin films," Cell Rep. Phys. Sci. **2**, 100596 (2021).
[63]T.-H. Li, V. Yadav, J. C. Conrad, and M. L. Robertson, "Effect of dispersity on the conformation of spherical polymer brushes," ACS Macro Lett. **10**, 518–524 (2021).
[64]W. Hu, *Polymer Physics: A Molecular Approach* (Springer Science & Business Media, 2012).
[65]A. Stukowski, "Visualization and analysis of atomistic simulation data with OVITO–the open visualization tool," Modell. Simul. Mater. Sci. Eng. **18**, 015012 (2009).
[66]X. Huang and C. B. Roth, "Optimizing the grafting density of tethered chains to alter the local glass transition temperature of polystyrene near silica substrates: The advantage of mushrooms over brushes," ACS Macro Lett. **7**, 269–274 (2018).
[67]W. Xia, J. Song, N. K. Hansoge, F. R. Phelan, Jr., S. Keten, and J. F. Douglas, "Energy renormalization for coarse-graining the dynamics of a model glass-forming liquid," J. Phys. Chem. B **122**, 2040–2045 (2018).
[68]A. Wang, F. Vargas-Lara, J. M. Younker, K. A. Iyer, K. R. Shull, and S. Keten, "Quantifying chemical composition and cross-link effects on EPDM elastomer viscoelasticity with molecular dynamics," Macromolecules **54**, 6780–6789 (2021).
[69]T. Prisk, M. Tyagi, and P. Sokol, "Dynamics of small-molecule glass formers confined in nanopores," J. Chem. Phys. **134**, 114506 (2011).
[70]W. Nie, J. F. Douglas, and W. Xia, "Competing effects of molecular additives and cross-link density on the segmental dynamics and mechanical properties of cross-linked polymers," ACS Eng. Au **3**, 512–526 (2023).
[71]J. Midya, Y. Cang, S. A. Egorov, K. Matyjaszewski, M. R. Bockstaller, A. Nikoubashman, and G. Fytas, "Disentangling the role of chain conformation on the mechanics of polymer tethered particle materials," Nano Lett. **19**, 2715–2722 (2019).
[72]W. Voigt, "Ueber die beziehung zwischen den beiden elasticitätsconstanten isotroper körper," Ann. Phys. **274**, 573–587 (1889).
[73]M. Jhalaria, Y. Cang, Y. Huang, B. Benicewicz, S. K. Kumar, and G. Fytas, "Unusual high-frequency mechanical properties of polymer-grafted nanoparticle melts," Phys. Rev. Lett. **128**, 187801 (2022).